ISSN1027-5495. Functional Materials, 32, No.1 (2025), p. 108-114
doi:http://dx.doi.org/10.15407/fm32.01.108

Effective polarizability and optical resonances of a square lattice of rod-like metal nanoparticles on a dielectric substrate

N.I. Pavlyshche[1], A.V. Korotun[1,2], V.P. Kurbatsky[1], R.Yu. Korolkov[1]

[1] National University "Zaporizhzhia Polytechnic" 64 University Str., Zaporizhzhia, 69063, Ukraine,
[2] G.V. Kurdyumov Institute for Metal Physics of National Academy of Sciences of Ukraine,
36 Academician Vernadsky Blvd., Kyiv, 03142, Ukraine

Received September 30, 2024

Resonance properties of the lattice of rod-like nanoparticles are studied in the local field approximation; the characteristics of single nanoparticles are calculated within the framework of the equivalent spheroid approach. According to the results of the calculations, a blue shift of the maxima of the imaginary part of the effective transverse polarizability for the square lattice of nanocylinders with a decrease in their effective aspect ratio was established. The imaginary part of the effective transverse polarization of the lattice of cylinders is four orders of magnitude greater than the corresponding value for a single cylinder. The lattice resonance frequency increases when metals with a higher plasma frequency are used or when the lattice is placed in a medium with a lower dielectric constant. The obtained results indicate a significant influence of the size, shape, and material of rod-like nanoparticles, as well as the surrounding medium, on the frequency dependence of the imaginary part of the effective transverse polarization of the lattice. The possibility of controlling the lattice resonance frequency by changing the effective aspect ratio of the nanoparticles forming the lattice has been demonstrated. The strong interaction between the constituent elements of the lattice leads to an increase by four orders of magnitude in the imaginary part of the effective transverse polarizability and the absorption cross section of the lattice in comparison with a single nanoparticle.

Keywords: effective polarizability, lattice resonance, lattice sums, effective relaxation rate.

Ефективна поляризовність та оптичні резонанси квадратної ґратки металевих стрижнеподібних наночастинок на діелектричній підкладці. *Н.І. Павлище, А.В. Коротун, В.П. Курбацький, Р.Ю. Корольков*

Резонансні властивості ґратки стрижнеподібних наночастинок досліджуються в наближенні локального поля, характеристики поодиноких наночастинок розраховуються в рамках підходу еквівалентного сфероїда. За результатами розрахунків встановлений синій зсув максимумів уявної частини ефективної поперечної поляризовності для квадратної ґратки наноциліндрів зі зменшенням їх ефективного аспектного відношення. Уявна частина ефективної поперечної поляризовності ґратки циліндрів на чотири порядки перевищує відповідну величину для поодинокого циліндра. Частота ґраткового резонансу збільшується при використанні металів із більшою плазмовою частотою або при розміщенні ґратки в середовищі з меншою діелектричною проникністю. Отримані результати свідчать про суттєвий вплив розмірів, форми і матеріалу стрижнеподібних наночастинок, а також оточуючого середовища на частотну залежність уявної частини ефективної поперечної поляризовності ґратки. Продемонстровано можливість керування частотою ґраткового резонансу шляхом зміни ефективного аспектного відношення наночастинок, що утворюють ґратку. Сильна взаємодія між складовими елементами ґратки призводить до збільшення на чотири порядки уявної частини ефективної поперечної поляризовності і перерізу поглинання ґратки у порівнянні з поодинокою наночастинкою.

1. Introduction

Oscillations of the conductivity electrons of a metal nanoparticle, excited by an external electromagnetic field, lead to the emergence of a localized surface plasmon resonance (SPR). During the resonance, the electric field in the region near the surface of the particle is amplified. The field amplification and the subwavelength nature of the localized SPR can be used to regulate the attenuation of the spontaneous radiation of nanoemitters [1], to control nonlinear effects such as second harmonic generation and Raman scattering [2,3]. However, due to strong radiation attenuation, SPRs have a large spectral line width and a low Q factor [4], which complicates their possible application.

If nanoparticles form an array, the interaction between them can cause additional resonances. In particular, when the period of the array is of the order of the resonance wavelength, the combination of diffraction on the array with the SPR of each individual particle leads to a collective resonance, which is called surface lattice resonance (SLR) [5–9].

The width of the surface lattice resonance lines in arrays of plasmonic nanoparticles depends on the angle of incidence and is much smaller than the width of the SPR line of an individual particle. These features make periodic arrays of metal nanoparticles attractive for practical applications and convenient for SLR setup. In particular, surface lattice resonance was used to collect light [10], to control radiation [11-13], to arrange a strong interaction of light with matter [14–16] and for plasmonic generation [9,17–20]. Recently, SLRs have been implemented in magnetoplasmonic responses of magnetic nanoparticle arrays [21, 22] upon excitation of the dark mode in arrays of asymmetric dimers [23] and superlattice plasmons in arrays of gold particles [24].

The optical properties of lattices of metal rod-like nanoparticles on a dielectric substrate depend on the characteristics of individual particles. Finding the frequency dependences of these characteristics is a non-trivial task, various aspects of which were considered in [25-28]. For description of nanoparticles of different shapes (elongated and flattened spheroids, cylinders, spherocylinders, discs, bicones, and bipyramids), the equivalent spheroid method was applied [29]. The results of the calculations are in good agreement with the experimental data, so the same approach is used in this work

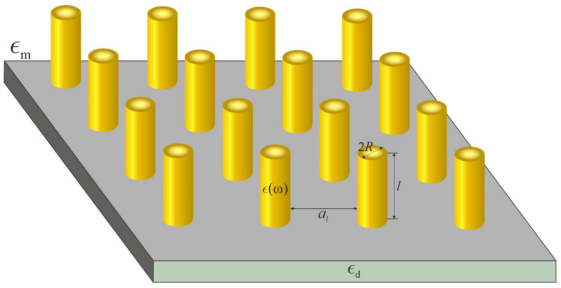

Fig. 1. Geometry of the problem

to find the characteristics of individual rod-like nanoparticles.

There are numerical models for calculating SLR characteristics, such as the discrete dipole approximation [30, 31], but there remains a need for transparent, understandable ways to determine the structure of SLR modes. Therefore, the study of resonant optical phenomena in lattices of rod-like metal nanoparticles is an urgent task.

2. Basic relationships

Let metal nanorods of length l and radius form a square lattice with the period a_l on a dielectric substrate with permeability ϵ_d (Fig. 1). The dielectric constant of the surrounding dielectric medium is ϵ_m. We apply the local field approximation [32] to study the optical properties of the system. In this approximation, under the condition of normal incidence of light on the substrate, the transverse component of the effective polarizability tensor of the lattice of rod-like nanoparticles is determined by the relation

$$\alpha_{latt}^{\perp} = \frac{\epsilon^{\perp}(\omega) - \epsilon_m}{\tilde{\mathcal{L}}_{\perp}\epsilon^{\perp}(\omega) + \left(1 - \tilde{\mathcal{L}}_{\perp}\right)\epsilon_m}, \qquad (1)$$

in which the renormalized depolarization factor has the form

$$\tilde{\mathcal{L}}_{\perp} = \mathcal{L}_{\perp} - \Phi_{\perp} V, \qquad (2)$$

where V is the volume of the rod-shaped nanoparticle,

$$\Phi_{\perp} = \frac{1}{a_l^3 \epsilon_m}\left(\mathcal{S}_{\perp}^{d} + \frac{\epsilon_d - \epsilon_m}{\epsilon_d + \epsilon_m}\mathcal{S}_{\perp}^{i}\right), \qquad (3)$$

$\mathcal{S}_{\perp}^{d}$ and $\mathcal{S}_{\perp}^{i}$ are lattice sums, which are determined by the interaction of the nanorods with each other and with the image dipoles.

The lattice sums are calculated according to the formulas [33]

$$\mathcal{S}_{\perp}^{d} = \sum_{n_x, n_y = -\infty}^{\infty} \frac{2n_x^2 - n_y^2}{\left(n_x^2 + n_y^2\right)^{5/2}}; \qquad (4)$$

Table 1. Geometrical parameters of rod-like nanoparticles (a and b are the major and minor semi-axes of the spheroid; R and l are the radius and length of the cylinder (spherocylinder)) [25]

Shape	Dimensions		Aspect ratio, ϱ	Effective aspect ratio, ϱ_{eff}	Volume, V
	longitudinal	transverse			
Prolate spheroid	$2a$	$2b$	b/a	ϱ	$\frac{4}{3}\pi ab^2$
Cylinder	l	$2R$	$2R/l$	$\frac{\sqrt{3}}{2}\varrho$	$\pi R^2 l$
Sphero-cylinder	$l+2R$	$2R$	$\frac{2R}{l+2R}$	$\left(1+\frac{4\delta}{3}\frac{\delta^2+\delta+\frac{3}{4}}{\delta+\frac{8}{15}}\right)^{-\frac{1}{2}}$, $\delta=1-\varrho$	$\pi R^2\left(l+\frac{4}{3}R\right)$

$$\mathcal{S}_{\perp}^{\,i}=\sum_{n_x,n_y=-\infty}^{\infty}\frac{-2n_x^2+n_y^2+(2z_0/a_l)^2}{\left(n_x^2+n_y^2+(2z_0/a_l)^2\right)^{5/2}} \quad (5)$$

where n_x and n_y are the numbers of rods in the two-dimensional lattice along the axes x and y; z_0 is the distance from the image dipoles to the surface of the substrate.

The most convenient is the method of calculating sums (4) and (5) using rapidly converging series. Representing the lattice sum (4) in the form

$$\mathcal{S}_{\perp}^{\,d}=2\sum_{n_x,n_y=-\infty}^{\infty}\frac{1}{\left(n_x^2+n_y^2\right)^{3/2}}-3\sum_{n_x,n_y=-\infty}^{\infty}\frac{n_y^2}{\left(n_x^2+n_y^2\right)^{5/2}} \quad (6)$$

and taking into account the known relations [33]

$$\sum_{n_x,n_y=-\infty}^{\infty}\frac{n_y^2}{\left(n_x^2+n_y^2\right)^{5/2}}=\frac{32\pi^2}{3}\sum_{m_x,m_y=1}^{\infty}m_x^2K_2\left(2\pi m_x m_y\right), \quad (7)$$

$$\sum_{n_x,n_y=-\infty}^{\infty}\frac{1}{\left(n_x^2+n_y^2\right)^{3/2}}=2\zeta(3), \quad (8)$$

we obtain

$$\mathcal{S}_{\perp}^{\,d}=4\left[\zeta(3)-8\pi^2\sum_{m_x,m_y=1}^{\infty}m_x^2K_2\left(2\pi m_x m_y\right)\right], \quad (9)$$

where $\zeta(z)$ is the Riemann zeta function, $\zeta(3)\approx 1{,}202$; $K_\nu(x)$ is the Macdonald function of the ν-th order.

Similarly, the lattice sum (5) written in the form

$$\mathcal{S}_{\perp}^{\,i}=\sum_{n_x,n_y=-\infty}^{\infty}\frac{1}{\left[n_x^2+n_y^2+\left(2z_0/a_l\right)^2\right]^{3/2}}-3\sum_{n_x,n_y=-\infty}^{\infty}\frac{n_x^2}{\left[n_x^2+n_y^2+\left(2z_0/a_l\right)^2\right]^{5/2}}, \quad (10)$$

if taking into account the relations [33]

$$\sum_{n_x,n_y=-\infty}^{\infty}\frac{1}{\left[n_x^2+n_y^2+\left(2z_0/a_l\right)^2\right]^{3/2}}=\frac{\pi a_l}{z_0}\sum_{m_x,m_y=1}^{\infty}\sqrt{m_x^2+m_y^2}\,K_1\left(4\pi\frac{z_0}{a_l}\sqrt{m_x^2+m_y^2}\right) \quad (11)$$

$$\sum_{n_x,n_y=-\infty}^{\infty}\frac{n_x^2}{\left[n_x^2+n_y^2+\left(2z_0/a_l\right)^2\right]^{5/2}}=\frac{1}{3}\left(\frac{\pi a_l}{z_0}\right)^2\sum_{m_x,m_y=1}^{\infty}m_x^2\left(m_x^2+m_y^2\right)K_2\left(4\pi\frac{z_0}{a_l}\sqrt{m_x^2+m_y^2}\right) \quad (12)$$

takes the form

$$\mathcal{S}_{\perp}^{\,i}=\frac{\pi a_l}{z_0}\sum_{m_x,m_y=1}^{\infty}\sqrt{m_x^2+m_y^2}\left\{K_1\left(4\pi\frac{z_0}{a_l}\sqrt{m_x^2+m_y^2}\right)-\frac{\pi a_l}{z_0}m_x^2\sqrt{m_x^2+m_y^2}\,K_2\left(4\pi\frac{z_0}{a_l}\sqrt{m_x^2+m_y^2}\right)\right\}. \quad (13)$$

In the equivalent spheroid method [25], the depolarization factors of rod-like nanoparticles are determined by the effective aspect ratio

(Table 1). This value is found from the condition of equality of the ratio of the longitudinal moment of inertia to the transverse one for a rod-shaped particle and an equivalent prolate spheroid. Expressions for depolarization factors have the form

$$\mathcal{L}_\perp = \frac{1}{2}\left(1-\mathcal{L}_\parallel\right);$$

$$\mathcal{L}_\parallel = \frac{\varrho_{\text{eff}}^2}{2\left(1-\varrho_{\text{eff}}^2\right)^{3/2}}\left(\ln\frac{1+\sqrt{1-\varrho_{\text{eff}}^2}}{1-\sqrt{1-\varrho_{\text{eff}}^2}}-2\sqrt{1-\varrho_{\text{eff}}^2}\right). \quad (14)$$

Within the framework of the Drude model, the transverse component of the dielectric tensor is

$$\epsilon^\perp(\omega) = \epsilon^\infty - \frac{\omega_p^2}{\omega\left(\omega+\mathrm{i}\gamma_{\text{eff}}^\perp\right)}, \quad (15)$$

where ϵ^∞ is the fraction of interband transitions in the dielectric function of the metal; ω_p is the plasma frequency; the transverse component of the effective relaxation rate has the form

$$\gamma_{\text{eff}}^\perp = \gamma_{\text{bulk}} + \gamma_{\text{surf}}^\perp + \gamma_{\text{rad}}^\perp. \quad (16)$$

In the right part of (16), the bulk relaxation rate $\gamma_{\text{bulk}} = \text{const}$; the surface relaxation rate and radiation attenuation are determined by the relations

$$\gamma_{\text{surf}}^\perp = \mathscr{A}_\perp \frac{v_{\text{F}}}{2R}, \quad (17)$$

$$\gamma_{\text{rad}}^\perp = \mathscr{B}_\perp \frac{v_{\text{F}}}{2R}, \quad (18)$$

with parameters

$$\mathscr{A}_\perp = \frac{9}{16}\frac{\mathcal{L}_\perp}{\epsilon_{\text{m}}+\mathcal{L}_\perp\left(1-\epsilon_{\text{m}}\right)}\left(\frac{\omega_p}{\omega}\right)^2 \mathscr{F}_\perp\left(\varrho_{\text{eff}}\right), \quad (19)$$

$$\mathscr{B}_\perp = \frac{9V}{128\pi}\frac{\mathcal{L}_\perp}{\sqrt{\epsilon_{\text{m}}\left[\epsilon^\infty+\left(\frac{1}{\mathcal{L}_\perp}-1\right)\epsilon_{\text{m}}\right]}}\left(\frac{\omega_p}{c}\right)^3\left(\frac{\omega_p}{\omega}\right)^2 \mathscr{F}_\perp\left(\varrho_{\text{eff}}\right), \quad (20)$$

where the size-dependent function appears [25]

$$\mathscr{F}_\perp\left(\varrho_{\text{eff}}\right) = \left(1-\varrho_{\text{eff}}^2\right)^{-\frac{3}{2}}\left\{2\left(\frac{3}{4}-\varrho_{\text{eff}}^2\right)\left(\frac{\pi}{2}-\arcsin\varrho_{\text{eff}}\right)+\varrho_{\text{eff}}\left(\frac{3}{2}-\varrho_{\text{eff}}^2\right)\sqrt{1-\varrho_{\text{eff}}^2}\right\} \quad (21)$$

Equating the real part of the denominator (1) to zero, we obtain an expression for the size dependence of the lattice resonance frequency of the nanorods array

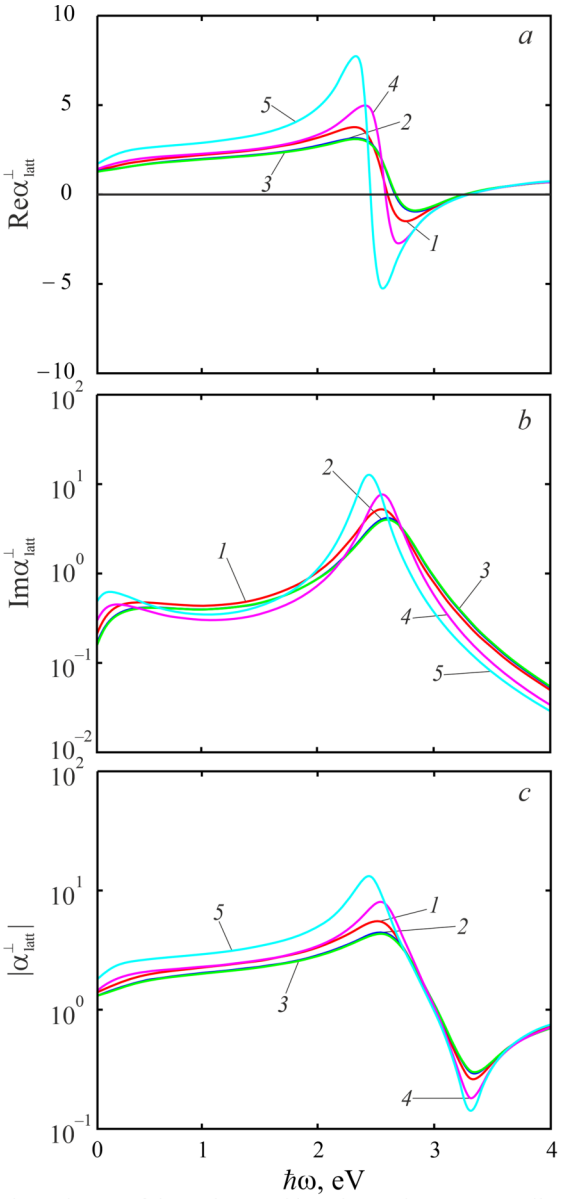

Fig. 2. Frequency dependences of the real (*a*) and imaginary (*b*) parts, as well as the modulus (*c*) of the transverse component of the lattice polarizability tensor for a square lattice of Au nanocylinders in Teflon: *1* – $r = 10$ nm, $l = 50$ nm; *2* – $r = 10$ nm, $l = 150$ nm; *3* – $r = 10$ nm; *4* – $r = 20$ nm, $l = 150$ nm; *5* – $r = 40$ nm, $l = 150$ nm.

$$\omega_{\text{res}}^{\text{latt},\perp} = \frac{\omega_p}{\sqrt{\epsilon^\infty+\frac{1-\tilde{\mathcal{L}}_\perp}{\tilde{\mathcal{L}}_\perp}\epsilon_{\text{m}}}}. \quad (22)$$

Further, relations (1) and (22) are used to obtain numerical results.

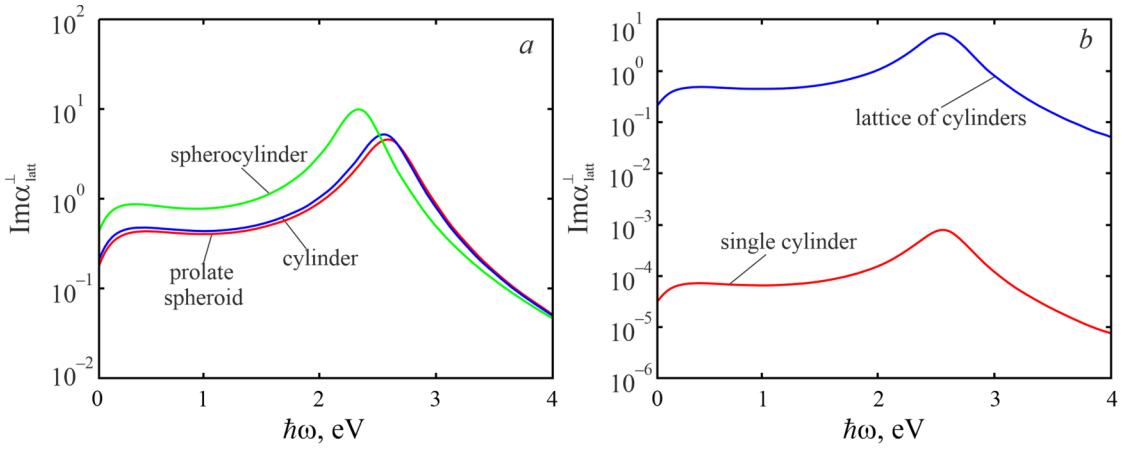

Fig. 3. Frequency dependences of the imaginary part of the transverse component of the polarizability tensor for lattices of Au nanoparticles of different shapes (*a*) and the lattice of cylindrical Au nanoparticles in comparison with a single cylinder (*b*) at the $r = 10$ nm, $l = 50$ nm

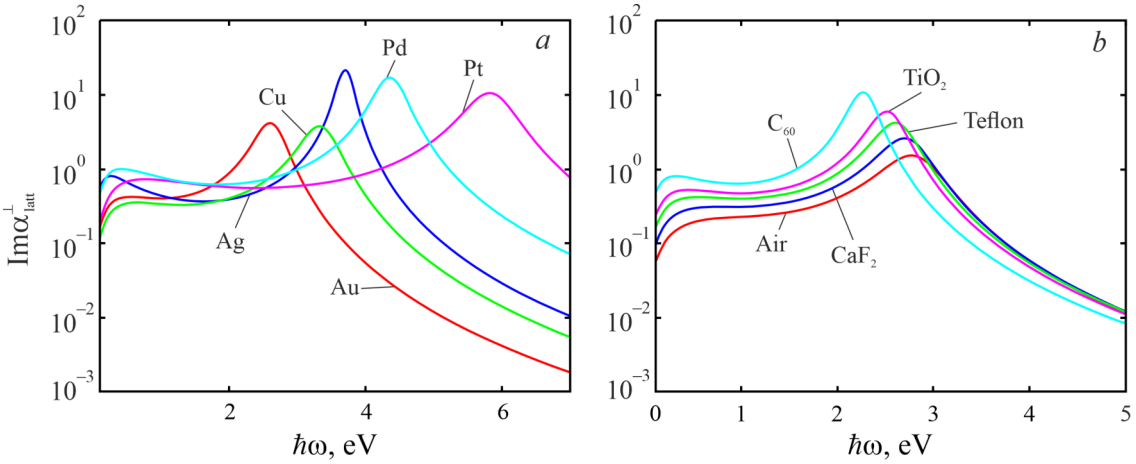

Fig. 4. Frequency dependences of the imaginary part of the transverse component of the polarizability tensor for lattices of nanoparticles of different metals in Teflon (*a*) and lattices of Au nanocylinders in different dielectrics (*b*) at the $r = 10$ nm, $l = 150$ nm

3. Results and discussion

Calculations were performed for rod-like metal nanoparticles of different sizes. The parameters of metals and permeability of dielectrics used in the calculations are given in Tables 2 and 3.

Fig. 2 shows the frequency dependences of the real and imaginary parts, as well as the modulus of the transverse component of the lattice polarizability tensor for a square lattice of Au nanocylinders. As in the case of single nanoparticles, $\mathrm{Re}\,\alpha^{\perp}_{latt}(\hbar\omega)$ is an alternating function, but $\mathrm{Im}\,\alpha^{\perp}_{latt}(\hbar\omega) > 0$ in the entire frequency interval studied. The results of the calculations demonstrate that the change in the size of the nanocylinders does not change the qualitative character of the frequency dependences, and the quantitative changes are insignificant. Thus, as the length increases, a slight decrease in the magnitude of the $\mathrm{Im}\,\alpha^{\perp}_{latt}(\hbar\omega)$

Table 2. Parameters of metals [25]

Metal	Parameter		
	ϵ^{∞}	$\hbar\omega_p$, eV	γ_{bulk}, 10^{13} s^{-1}
Pd	2.52	9.7	13.9
Ag	3.70	9.17	2.50
Pt	4.42	15.2	10.52
Au	9.84	9.07	3.45
Cu	12.03	12.6	3.70

Table 3. Dielectric permeability of the substrate (ϵ_d) and matrix (ϵ_m) [25]

Substrate	Matrix				
SiO_2	Air	CaF_2	Teflon	TiO_2	C_{60}
2.25	1.0	1.54	2.3	4.0	6.0

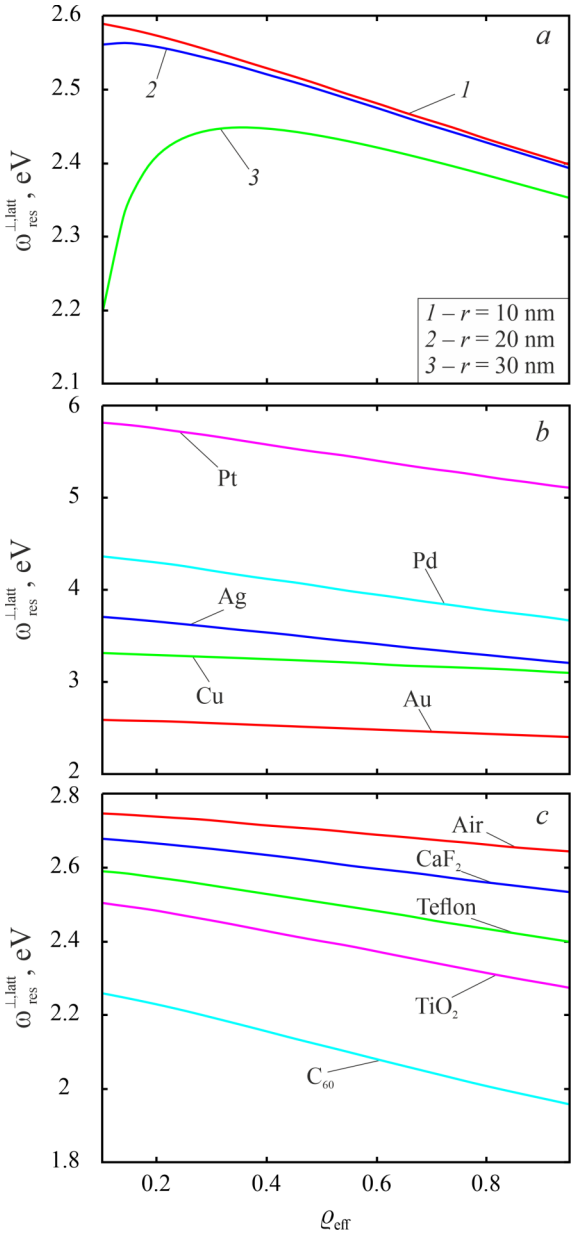

Fig. 5. Size dependences of the lattice resonance frequency for lattices of Au nanocylinders of different radii (*a*), different metals (*b*) and in different media (*c*)

function maxima, accompanied by their small blue shift. In turn, an increase in the radius of a cylinder results in a red shift of the maxima and an increase in their magnitude. Therefore, a decrease in the effective aspect ratio leads to a blue shift with a simultaneous decrease in their magnitude.

Fig. 3*a* demonstrates the similarity of the frequency dependences of the imaginary part of the transverse component of the polarizability tensor for lattices of different rod-shaped Au nanoparticles. The frequency dependences in Fig. 3*b* indicate that the SPR frequency for a single cylinder and the SLR frequency for a lattice of nanocylinders practically coincide, while the ratio $\mathrm{Im}\,\alpha_{\mathrm{latt}}^{\perp}/\mathrm{Im}\,\alpha_{\mathrm{cyl}}^{\perp} \cong 10^4$; this fact can be explained by the strong interaction of nanocylinders in the lattice.

The frequency dependences of the imaginary part of the transverse component of the effective polarizability tensor for lattices of nanocylinders of different metals and a lattice of Au nanocylinders in different dielectric media are shown in Fig. 4. For cylinders of different metals, the location of $\max\left\{\mathrm{Im}\,\alpha_{\mathrm{latt}}^{\perp}\right\}$, which correspond to SLR frequencies, are determined by plasma frequencies. For a lattice of nanocylinders in different dielectric media, the frequency dependence maxima shift toward lower frequencies as the permeability of the medium increases.

Fig. 5 shows the dependences of the lattice resonance frequency on the effective aspect ratio for lattices of Au nanocylinders of different radius (*a*), different metals (*b*), located in different dielectrics (*c*). Note that at a fixed value of the effective aspect ratio, the SLR frequency increases with an increase in the plasma frequency of the metal and a decrease in the permeability of the medium. The last fact can be proved by calculating the derivative of $\omega_{\mathrm{res}}^{\mathrm{latt},\perp}$ with respect to ϵ_{m}:

$$\frac{\partial\omega_{\mathrm{res}}^{\mathrm{latt},\perp}}{\partial\epsilon_{\mathrm{m}}} = -\frac{1}{2}\omega_p\left(\epsilon^{\infty}+\frac{1-\tilde{\mathcal{L}}_{\perp}}{\tilde{\mathcal{L}}_{\perp}}\epsilon_{\mathrm{m}}\right)^{-3/2}\times \tag{23}$$

$$\times\left\{\frac{1-\tilde{\mathcal{L}}_{\perp}}{\tilde{\mathcal{L}}_{\perp}}-\frac{V}{a_l^3\epsilon_{\mathrm{m}}\tilde{\mathcal{L}}_{\perp}^2}\left[\mathcal{S}_{\perp}^{\,d}+\mathcal{S}_{\perp}^{\,i}\left(1-2\left(\frac{\epsilon_{\mathrm{m}}}{\epsilon_{\mathrm{d}}+\epsilon_{\mathrm{m}}}\right)^2\right)\right]\right\}<0,$$

since

$$\frac{1-\tilde{\mathcal{L}}_{\perp}}{\tilde{\mathcal{L}}_{\perp}} > \frac{V}{a_l^3\epsilon_{\mathrm{m}}\tilde{\mathcal{L}}_{\perp}^2}\left[\mathcal{S}_{\perp}^{\,d}+\mathcal{S}_{\perp}^{\,i}\left(1-2\left(\frac{\epsilon_{\mathrm{m}}}{\epsilon_{\mathrm{d}}+\epsilon_{\mathrm{m}}}\right)^2\right)\right].$$

4. Conclusions

In the approximation of the local field, expressions for the frequency dependence of the transverse component of the effective polarizability tensor and the size dependence of the resonance frequency of a square lattice of metal rod-like nanoparticles located on a dielectric substrate were obtained.

It was established that with a decrease in the effective aspect ratio, there is a decrease in the height of the spectral maxima of the imaginary part of the transverse component of the effective polarizability and their blue shift.

The strong interaction of nanocylinders in the lattice leads to a sharp increase in the value of the imaginary part of the transverse effective polarizability of the lattice in comparison with its value for a single nanocylinder.

The calculated dependences of the lattice resonance frequency on the effective aspect ratio (size dependence) for lattices of nanocylinders of different metals and in different media demonstrate a monotonous decrease in frequency with an increase in the aspect ratio in all cases. At a fixed value of the effective aspect ratio, the lattice resonance frequency increases with an increase in the plasma frequency of the metal and a decrease in the permeability of the medium.

References

1. P. Anger, P. Bharadwaj, and L. Novotny, *Phys. Rev. Lett.*, **96**, 113002 (2006).
2. K.A. Willets and R.P. Van Duyne, *Annu. Rev. Phys. Chem.*, **58**, 267 (2007).
3. L. Chu, Z. Li, H. Zhu, F. Ren, and F. Chen, *Appl. Phys. Lett.*, **120**, 073104 (2022).
4. A.V. Korotun, H.V. Moroz, and R.Yu. Korolkov, *Funct. Mater.*, **31**, 119–127 (2024).
5. V. G. Kravets, F. Schedin, A. N. Grigorenko, *Phys. Rev. Lett.*, **101**, 087403 (2008).
6. B. Auguié and W.L. Barnes, *Phys. Rev. Lett.*, **101**, 143902 (2008).
7. S.R.K. Rodriguez, A. Abass, B. Maes, O.T.A. Janssen, G. Vecchi, and J.G. Rivas, *Phys. Rev. X*, **1**, 021019 (2011).
8. N. Meinzer, W. L. Barnes, and I. R. Hooper, *Nat. Photonics*, **8**, 889 (2014).
9. D. Dey, G. C. Schatz, *MRS Bull.*, **49**, 421 (2024).
10. Z. Li, S. Butun, and K. Aydin, *ACS Nano*, **8**, 8242 (2014).
11. G. Vecchi, V. Giannini, and J. G. Rivas, *Phys. Rev. Lett.*, **102**, 146807 (2009).
12. S. R. K. Rodriguez, G. Lozano, M. A. Verschuuren, R. Gomes, K. Lambert, B. D. Geyter, A. Hassinen, D. V. Thourhout, Z. Hens, and J. G. Rivas, *Appl. Phys. Lett.*, **100**, 111103 (2012).
13. R. Guo, S. Derom, A. I. Väkeväinen, R. J. A. van Dijk-Moes, P. Liljeroth, D. Vanmaekelbergh, and P. Törmä, *Opt. Express*, **23**, 28206 (2015).
14. P. Törmä and W. L. Barnes, *Rep. Prog. Phys.*, **78**, 013901 (2015).
15. A. I. Väkeväinen, R. J. Moerland, H. T. Rekola, A.-P. Eskelinen, J.-P. Martikainen, D.-H. Kim, P. Törmä, *Nano Lett.*, **14**, 1721 (2014).
16. L. Shi, T. K. Hakala, H. T. Rekola, J.-P. Martikainen, R. J. Moerland, P. Törmä, *Phys. Rev. Lett.*, **112**, 153002 (2014).
17. J. Stehr, J. Crewett, F. Schindler, R. Sperling, G. von Plessen, U. Lemmer, J. Lupton, T. Klar, J. Feldmann, A. Holleitner, M. Forster, U. Scherf, *Adv. Mater.*, **15**, 1726 (2003).
18. W. Zhou, M. Dridi, J. Y. Suh, C. H. Kim, D. T. Co, M. R. Wasielewski, G. C. Schatz, T. W. Odom, *Nat. Nanotechnol.*, **8**, 506 (2013).
19. X. Meng, J. Liu, A. V. Kildishev, V. M. Shalaev, *Laser Photon. Rev.*, **8**, 896 (2014).
20. T. K. Hakala, H. T. Rekola, A. I. Väkeväinen, J.-P. Martikainen, M. Necada, A. J. Moilanen, and P. Törmä, *Nat. Commun.*, **8**, 13687 (2017).
21. N. Maccaferri, X. Inchausti, A. García-Martín, J. C. Cuevas, D. Tripathy, A. O. Adeyeye, P. Vavassori, *ACS Photonics*, **2**, 1769 (2015).
22. L. Cerdán, J. R. Deop-Ruano, J. J. Alvarez-Serrano, A. Manjavacas, *Adv. Opt. Mater.*, **12**, 2302737 (2024).
23. A. D. Humphrey, N. Meinzer, T. A. Starkey, W. L. Barnes, *ACS Photonics*, **3**, 634 (2016).
24. D. Wang, A. Yang, A. J. Hryn, G. C. Schatz, T. W. Odom, *ACS Photonics*, **2**, 1789 (2015).
25. A. V. Korotun, Ya. V. Karandas, V. I. Reva, *Ukr. J. Phys.*, **67**, 849–858 (2022).
26. A. V. Korotun and N. I. Pavlyshche, *Funct. Mater.*, **29**, 567–575 (2022).
27. A.O. Koval, *J. of Nano- Electron. Phys.*, **15**, 01014 (2023).
28. A. V. Korotun, *Ukr. J. Phys.*, **68**, 695–704 (2023).
29. D. Constantin, *Eur. Phys. J. E*, **38**, 116 (2015).
30. G. Schatz, *J. Mol. Struct. THEOCHEM*, **573**, 73 (2001).
31. K. L. Kelly, E. Coronado, L. L. Zhao, and G. C. Schatz, *J. Phys. Chem. B*, **107**, 668 (2003).
32. V. A. Kosobukin, *Phys. Solid State*, **54**, 2471–2480 (2012).
33. J. M. Borwein, M. L. Glasser, R. C. McPhedran, J. G. Wan, and I. J. Zucker, *Lattice Sums Then and Now* (Cambridge University Press, 2013).